Barrierless reactions between two closed-shell molecules. I. Dynamics of F 2 + C H 3 S C H 3 reaction

Yu-Ju Lu, Lance Lee, Jun-Wei Pan, Tingxian Xie, Henryk A. Witek, and Jim J. Lin

Citation: The Journal of Chemical Physics **128**, 104317 (2008); doi: 10.1063/1.2837801
View online: http://dx.doi.org/10.1063/1.2837801
View Table of Contents: http://scitation.aip.org/content/aip/journal/jcp/128/10?ver=pdfcov
Published by the AIP Publishing

Barrierless reactions between two closed-shell molecules. I. Dynamics of $F_2+CH_3SCH_3$ reaction

Yu-Ju Lu,[1] Lance Lee,[1,2] Jun-Wei Pan,[1] Tingxian Xie,[1,3] Henryk A. Witek,[4] and Jim J. Lin[1,4,a)]

[1]*Institute of Atomic and Molecular Sciences, Academia Sinica, Taipei 10617, Taiwan*
[2]*Department of Chemistry, National Taiwan University, Taipei 10617, Taiwan*
[3]*Department of Physics, Dalian Jiaotong University, Dalian 116028, China*
[4]*Department of Applied Chemistry, National Chiao Tung University, Hsinchu 30010, Taiwan and Institute of Molecular Science, National Chiao Tung University, Hsinchu 30010, Taiwan*

(Received 4 December 2007; accepted 4 January 2008; published online 14 March 2008)

A detailed experimental and theoretical investigation of the first-reported barrierless reaction between two closed-shell molecules [J. Chem. Phys. **127**, 101101 (2007)] is presented. The translational energy and angular distributions of two product channels, $HF+CH_2SFCH_3$ and $F+CH_3SFCH_3$, determined at several collision energies, have been analyzed to reveal the dynamics of the studied reaction. Detailed analysis of the experimental and computational results supports the proposed reaction mechanism involving a short-lived $F-F-S(CH_3)_2$ intermediate, which can be formed without any activation energy. Other possible reaction mechanisms have been discriminated. The decay of the intermediate and competition between the two product channels have been discussed. © *2008 American Institute of Physics*. [DOI: 10.1063/1.2837801]

I. INTRODUCTION

It is a widely accepted concept that radicals are more reactive than molecules, especially for molecules of closed-shell electronic character. Mechanistic studies of elementary reactions between two closed-shell molecules are much more challenging, mostly due to small reaction rate constants.[1] As a result, in the literature there are very few investigations of mechanism of molecule-molecule reactions, in contrast to numerous studies of radical-molecule reactions. In a recent study,[2] we have demonstrated an unusual type of chemical interaction between two closed-shell molecules, F_2 and CH_3SCH_3 [(DMS) dimethyl sulfide]. Two primary product channels have been identified with the crossed molecular beam technique,

$$\text{(I)}\quad F_2 + CH_3SCH_3 \rightarrow HF + CH_2{=}S(F){-}CH_3,$$

$$\text{(II)}\quad \rightarrow F + CH_3{-}S(F){-}CH_3.$$

As detailed calculations will show later, the reaction enthalpies of these channels are $\Delta H^{\circ}_{0\ K}(\text{I}) = -80.1$ kcal/mol and $\Delta H^{\circ}_{0\ K}(\text{II}) = 3.4$ kcal/mol.

For this reaction, the collision energy dependences of the reaction cross section and branching ratio have been investigated. All experimental results are consistent with the model of a weakly bound $F-F-S(CH_3)_2$ intermediate,[2] which possesses a special type of three-center four-electron bonds.[3] Remarkably, this intermediate can be formed without activation energy. A clear evidence for this conclusion is that the experimental cross section of channel I increases when the collision energy is reduced. On the other hand, collision energy larger than 6 kcal/mol is needed for observing the products of the endothermic channel II.[2] In previous crossed molecular beam studies, it was found that F_2 does react with some iodine compounds (I_2, ICl, HI, CH_3I (Refs. 4–9) and unsaturated hydrocarbons (C_2H_4, C_6H_6).[10,11] In these reactions, however, only a process analogous to channel II was observed with a significant threshold for collision energy. The high reactivity between F_2 and DMS is unusual for a typical molecule-molecule interaction, yet it may be quite general for the reactions of F_2 with molecules having a loosely bound lone pair of electrons.

Turnipseed and Birks[12] investigated the kinetics of F_2+DMS reaction in a flow tube with mass spectrometry and infrared emission spectroscopy. Strong chemiluminescence was observed in the reaction system. The emitting species were identified as HF, H_2CS, HCF, etc. Production of atomic fluorine was observed via the detection of FCl after adding excess Cl_2 in the reaction mixture ($Cl_2+F \rightarrow FCl+Cl$). Once the reaction is initiated, the production of F atom (or other radicals) can create an exothermic chain of reactions, which produces excited-state species responsible for the chemiluminescence. The room temperature rate constant of F_2+DMS reaction was measured to be $1.6 \pm 0.5 \times 10^{-11}$ cm^3 molecule^{-1} s^{-1}. The authors suggested that this unusually large rate constant correlates with the stability of the $[CH_3SCH_3]^+[F_2]^-$ ion pair; this conclusion was drawn after measuring the chemiluminescence intensity for a series of reactants. Turnipseed and Birks also detected a product with a mass-to-charge ratio of 80 amu/e, which is likely to be the CH_2SFCH_3 product (channel I) observed in our study.[2] Baker *et al.*[13] studied the same reaction by vacuum UV photoelectron spectroscopy under similar flow tube conditions, in which an intermediate species was detected in early reaction times with a vertical ionization energy of 8.03 ± 0.02 eV and tentatively assigned to CH_3SFCH_3. This

a)Electronic mail: jimlin@gate.sinica.edu.tw.

observation is consistent with our results for channel II. Other products such as H_2CS, H_2CCS, CH_3SH, HFCS, and HCF were observed for longer reaction times. Although many products were observed in those bulk experiments,[12,13] most of them are actually secondary—or even tertiary—products formed in multiple steps of reactions. As mentioned in Ref. 12, due to the large variety of possible products, it is not possible to isolate any distinct reaction steps under these conditions.

In this paper we report a detailed investigation of the $F_2+CH_3SCH_3$ reaction using the crossed molecular beam technique. The capability of identifying primary products with the crossed molecular beam technique can greatly simplify the task of deducing reaction mechanism.[14] In addition, we present high level *ab initio* calculations that offer a convenient framework to analyze the experimental results and provide a consistent picture of the reaction pathways.

II. METHODS

A. Crossed beam experiments

The crossed molecular beam apparatuses have been described previously.[15,16] Here, only the relevant experimental setup is given. Both molecular beams were generated from expansion through a fast pulsed valve[17] (Even-Lavie valve, high repetition rate model, $\leqslant$1000 Hz) and collimated by a sharp-edge skimmer (Beam Dynamics, Inc.). To vary the collision energy, various seeding ratio (5%–100%) in different noble gases (He, Ne, and/or Ar) was used for both molecular beams. The nozzle of the DMS beam source could be heated to about 400 K to reduce cluster formation, which was monitored by a mass spectrometer and controlled to be negligible. The nozzle of the F_2 beam source could be cooled to 150 K to reduce the beam speed.

The two reactant beams crossed each other at an angle of 90°. After traveling a fixed flight distance, the scattered products were detected with a time-resolved quadruple mass spectrometer. Here, the short pulse of the F_2 molecular beam ($\sim$15 μs) was used to define the starting time of the collision event. To reduce the background, the ionizer of the mass spectrometer was located in a differentially pumped chamber maintained at ultrahigh vacuum (10^{-11} torr). Time-of-flight (TOF) spectra of the products were recorded with a multichannel scalar (EG&G Ortec, Turbo MCS). The TOF distributions collected at different detector angles were integrated to give a laboratory angular distribution. Speed distributions of the molecular beams were measured with a fast rotating chopper wheel.

Two kinds of ionization methods, electron impact ionization and vacuum UV photoionization, were used in the experiment. The vacuum UV photon beam was provided from the synchrotron radiation from the 9 cm undulator beamline[18] of the Taiwan Light Source. The light intensity is about 10^{16} photon/s; it is tunable in the range from 8 to 21 eV with a 3% bandwidth. The electron impact apparatus[15] has a longer flight path of 24.2 cm in comparison with the 10.1 cm in the synchrotron apparatus.[16] For better velocity resolution, the analysis of the TOF spectra is based on the electron impact results.

In some experiments, CD_3SCD_3 (d6-DMS, 99%d, Aldrich Inc.) was used to shift the masses of the products, and thus to avoid overlapping with background masses from impurity of the commercial DMS sample. If necessary, the impurity contribution from the DMS beam could be adequately reproduced by performing Ar+DMS scattering experiments under similar conditions. We did not observe any significant isotope effect in most experimental aspects, including the reaction thresholds, TOF and angular distributions, and product photoionization spectra.

To transform the data measured in the laboratory (LAB) frame to the center-of-mass (CM) frame, we used a forward convolution method to include the instrument functions, such as velocity spreads of the molecular beams, spread of the flight length, etc. The LAB-frame TOF spectra and angular distributions were simulated using a computer program, which used a set of trial CM-frame angular distribution $P(\theta_{CM})$ and translational energy distribution $P(E_T)$ as an input. The $P(\theta_{CM})$ and $P(E_T)$ curves were iteratively adjusted until a satisfactory fit to the experimental data could be obtained. The factor of the LAB-CM transformation Jacobian was included in the program.

For experiments at low collision energies, slow molecular beams have to be used because our apparatuses have a fixed crossing angle of 90°. Here, we used an effusivelike DMS molecular beam instead of a usual supersonic one to achieve lower speeds. A fast chopper wheel ($\leqslant$400 s^{-1}) was installed at the exit of the pulsed valve to clearly define the opening time. After traveling 60 mm, fast and slow components of the DMS beam separate in time. Crossing with the short pulse of the F_2 beam serves as a velocity selector, in which only a given velocity component of the DMS beam collides with the F_2 beam. In this way, we can vary the collision energy by tuning the relative delay time between the two molecular beam sources. The intensity of the DMS beam could be measured with a fast ionization gauge (Beam Dynamics, Inc.). After colliding with the F_2 beam, the DMS beam was slightly ($\sim$10%) attenuated. The intensity of the F_2 beam could be deduced from the amount of attenuation. For determining the relative reaction cross section, the signal (after including the factor of the LAB-CM transformation Jacobian) has been normalized with respect to the F_2 and DMS beam intensities.

B. *Ab initio* calculations

To adequately reproduce chemical interactions between the reacting subsystems, complete-active-space self-consistent-field (CASSCF) calculations with the second-order multireference perturbation theory (CASPT2) (Refs. 19 and 20) corrections have been used to probe the potential energy surface along the reaction coordinate. All calculations have been performed without taking into account molecular symmetry, i.e., using the C_1 symmetry point group. This setting allows us to avoid unnecessary bias in choosing active orbitals. The employed active spaces have been carefully chosen and tested. Dunning basis sets[21,22] (cc-pVNZ and aug-cc-pVNZ, $N=T,Q,5$) have been used. It is clear that the atoms playing major role in the F_2+DMS reaction are fluo-

rine and sulfur. Therefore, we have tested a few types of basis sets for the S and F atoms. Since some of the studied species display large dipole moments—with the negative charge located at fluorine—we have chosen the aug-cc-pVNZ basis sets for the F atoms. This choice has been motivated by the fact that negatively charged ions usually require augmented basis sets to appropriately describe diffuse character of the anions.[22] The use of the augmented basis sets has allowed us to reproduce well the electron affinity of fluorine, in contrast to the calculations performed without additional diffuse basis functions. Additional tight *d* functions[23] have been used for the S atom to describe the non-Lewis character of sulfur in most of the studied structures. For C and H, we have found that the relative energies and geometries change only very little when the cc-pVDZ (double zeta) basis sets are replaced by the cc-pVTZ (triple zeta) basis sets. This observation indicates that the size of basis sets is less crucial for a proper description of the methyl groups, especially when they display similar electronic structure in both initial and final states. The presented geometry optimization and reaction-path calculations have used the following scheme of basis sets: cc-pVDZ for C and H, cc-pV(T+d)Z for S, and aug-cc-pVTZ for F. Larger basis sets, up to quintuple zeta (-cc-pV5Z), have been used for calculating single-point energies using the CCSD(T) and QCISD(T) methods.[24] In the situations where the QCISD(T) analytical gradients[25] are available, QCISD(T) has also been used for the geometry optimization. All the calculations have been performed with the MOLPRO 2006.1 quantum chemistry package.[26]

III. RESULTS AND DISCUSSION

A. Crossed beam experiments

The CH_2SFCH_3 product has been observed at mass 80 (the parent ion) and mass 65 (a daughter ion) with the electron impact detection. Figure 1 shows the TOF spectra of mass 80 at 10.0 kcal/mol collision energy. It is clear that the signal is more intense at LAB angles closer to the DMS beam direction. The corresponding CM-frame angular distribution $P(\theta_{CM})$ and translational energy distribution $P(E_T)$ used to fit to the TOF spectra are shown in Fig. 2. At this collision energy, the $P(\theta_{CM})$ shows a very significant forward peak and a quite weak backward peak. A worse but acceptable fit can be obtained if we remove the small backward peak. One $P(E_T)$ distribution is used for all θ_{CM} angles. If we allow different $P(E_T)$ distributions at different θ_{CM} angles, a better fit can be obtained. However, the difference between the two fitting schemes is not very significant. For simplicity reason, here we present the one $P(E_T)$ results for both channels I and II.

Figure 3 shows the TOF spectra of mass 85 (CD_2SFCD_3) product from $F_2+CD_3SCD_3$ crossed beam reaction at 7.3 kcal/mol collision energy. We have not observed any significant isotope effect due to the deuterium substitution. A single set of $P(\theta_{CM})$ and $P(E_T)$ can fit both h6-DMS and d6-DMS reactions provided the collision energy is similar. Figure 4 shows the product TOF spectra at mass 65 from the $F_2+CH_3SCH_3$ crossed beam reaction at

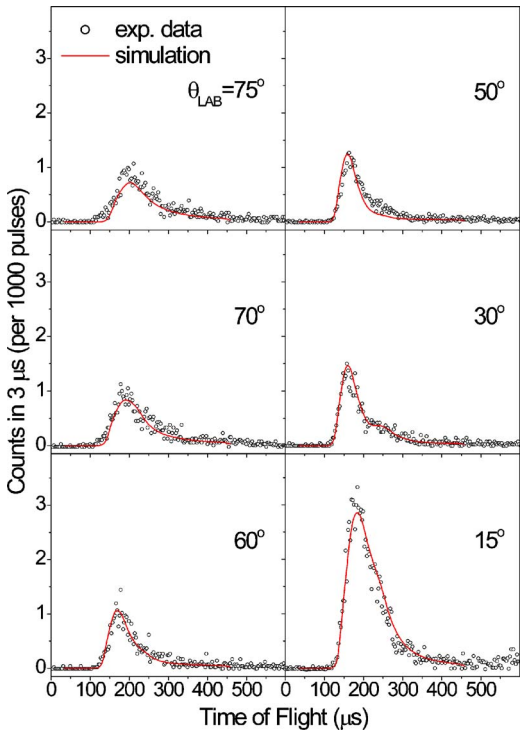

FIG. 1. (Color online) TOF spectra of the mass 80 product (CH_2SFCH_3) at selected LAB angles. The collision energy is 10.0 kcal/mol. The direction of the DMS molecular beam in the LAB-frame corresponds to 0° and the direction of the F_2 beam to 90°.

2.4 kcal/mol. Here the mass 65 (CH_2SF^+), a daughter ion of CH_2SFCH_3, has been chosen to avoid background from the scattered impurity in the commercial sample. We have checked the signals at mass 80 and 65 at several LAB angles. After background subtraction, they display the same TOF

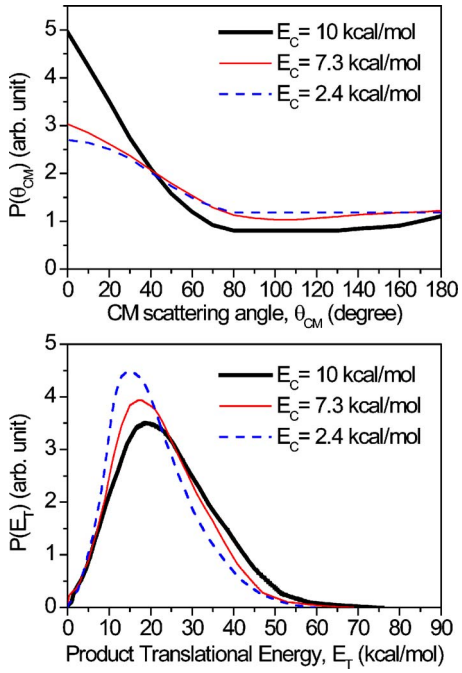

FIG. 2. (Color online) The CM-frame angular distribution $P(\theta_{CM})$ and translational energy distribution $P(E_T)$ used to simulate the LAB-frame TOF spectra and angular distributions for the channel I products.

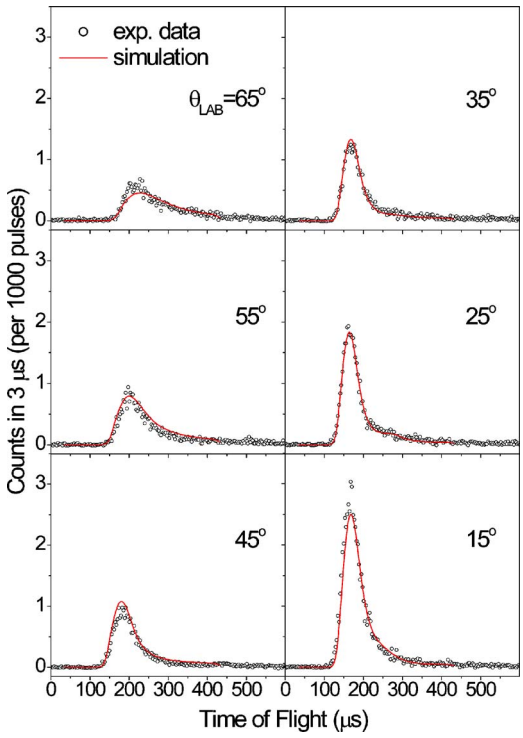

FIG. 3. (Color online) TOF spectra of mass 85 (CD_2SFCD_3) obtained for the $F_2+CD_3SCD_3$ crossed beam reaction at 7.3 kcal/mol collision energy.

spectra and angular distributions, indicating that the mass 65 signal can well represent the CH_2SFCH_3 product.

In Fig. 2, all $P(E_T)$ curves extend to a high energy of about 60 kcal/mol, consistent with the large exothermicity of channel I. We can also see that the $P(E_T)$ has a small dependence on the collision energy, which may be expected because the collision energy is only a small fraction of the available energy. The peak values of the $P(E_T)$ distributions are about 20 kcal/mol or less, indicating that major part (~75% in average) of the available energy is deposited into the internal degrees of freedom of the $HF+CH_2SFCH_3$ product pair. For F_2+DMS reaction, Turnipseed and Birks observed infrared emission from high vibrational states of HF in the flow tube condition.[12] However, they could not distinguish between emission from the primary products and from the secondary products. The later may be produced, for example, in the $H+F_2 \rightarrow HF\ (v \leqslant 9)+F$ reaction.

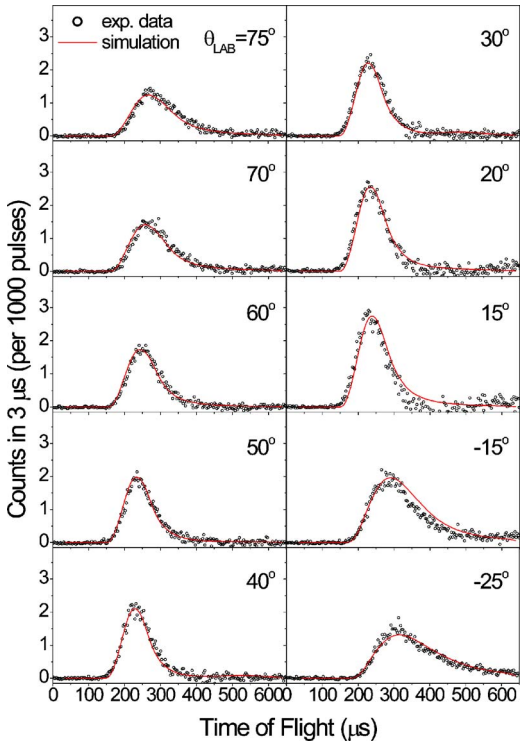

FIG. 4. (Color online) TOF spectra of mass 65 (CH_2SF^+) obtained for the $F_2+CH_3SCH_3$ crossed beam reaction at 2.4 kcal/mol. CH_2SF^+, a daughter ion of CH_2SFCH_3, has been chosen to avoid background interference.

The angular distribution has more significant dependence on the collision energy. At high collision energies (e.g., 10 kcal/mol), $P(\theta_{CM})$ shows a pronounced forward peak. This peak becomes smaller for lower collision energies. For this reaction, we have not observed a forward-backward symmetric angular distribution—a typical signature of a long-lived intermediate with lifetime substantially longer than its rotational period.[27] Since the reaction barrier is negligible,[2] collisions at large impact parameters should be the major contribution to the reaction cross section. Such collisions usually lead to a forward-peaking product distribution for a direct reaction (a reaction without significant time delay).[27] However, the extent of the forward peak depends on the collision energy, suggesting a mechanism of an osculating complex.[28] At high collision energies, the reaction is fast and the lifetime of the complex is substantially shorter than its rotational period, leading to a strongly forward-peaking angular distribution. At lower collision energies, the lifetime of the complex is longer and may eventually become more comparable to one rotational period. In the case of a polyatomic reaction, longer lifetime allows the relative contribution of the in-plane and out-of-plane angular motions, which may lead to a less forward-peaking and more isotropiclike distribution.[29] In the osculating complex model, the rotational period can be used as an internal clock, even though it depends weakly on the collision energy. Nevertheless, the reaction rate has usually much stronger energy dependence. Thus, for higher collision energies, the increase of the reaction rate exceeds the increase of the rotational frequency by quite a significant factor, such that the forward peak becomes more pronounced for the channel I product in the F_2+DMS reaction.

Channel II has been observed to be a minor product channel in the studied reaction. Its branching ratio depends strongly on the collision energy with an experimental threshold of 6 kcal/mol.[2] Figure 5 shows the TOF spectra of the mass 87 product from $F_2+CD_3SCD_3$ reaction at 11 kcal/mol collision energy. Besides the main signal peak (CD_3SFCD_3 of channel II), a small additional feature can be observed in shorter TOF. This additional feature can be assigned as the ^{34}S contribution of the CD_2SFCD_3 product (channel I), which is consistent with the TOF spectrum at mass 85 and the natural abundance of sulfur isotopes ($^{34}S/^{32}S=4.5\%$). The $P(E_T)$ and $P(\theta_{CM})$ used to fit the TOF spectra and angular distribution for channel II are shown in Fig. 6. Similarly like in the fitting scheme of channel I, only one $P(E_T)$ has been used for simplicity. The $P(E_T)$ has a maximum at

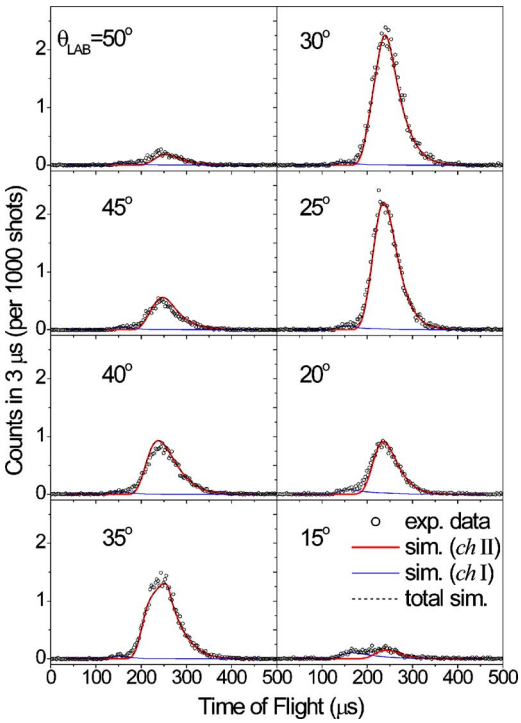

FIG. 5. (Color online) TOF spectra of the mass 87 products obtained for the $F_2+CD_3SCD_3$ reaction at 11 kcal/mol collision energy. In addition to the main signal peak (CD_3SFCD_3 of channel II), a faster peak from the ^{34}S contribution of the CD_2SFCD_3 product (channel I) can be seen.

low energy (about 1.5 kcal/mol) suggesting a small exit barrier for this process, which possibly corresponds to a centrifugal barrier resulting from collisions at nonzero impact parameters. The $P(\theta_{CM})$ is forward peaking, similar to that of channel I. The $P(E_T)$ and $P(\theta_{CM})$ used to fit the experimental results at 7.3 kcal/mol are also shown in Fig. 6 for comparison. However, the fitting at 7.3 kcal/mol is less accurate than that at 11 kcal/mol for two reasons. The signal at

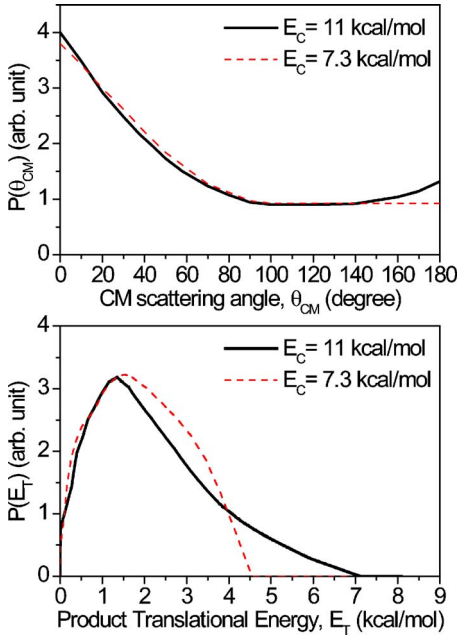

FIG. 6. (Color online) $P(E_T)$ and $P(\theta_{CM})$ used to simulate the TOF and angular distributions for the channel II products.

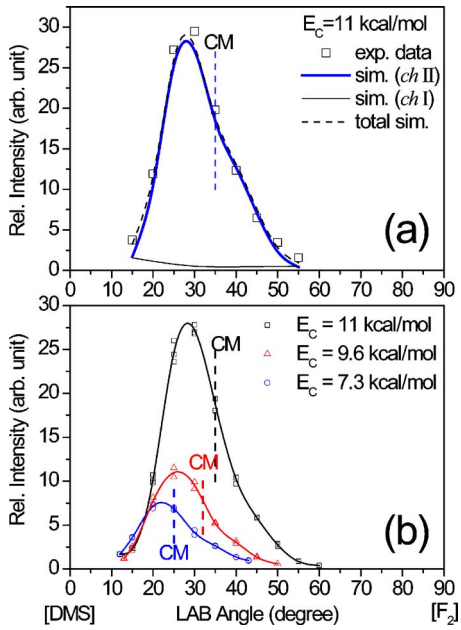

FIG. 7. (Color online) Typical LAB-frame angular distributions of channel II products: (a) experimental data and simulation at 11.0 kcal/mol collision energy and (b) experimental data (points together with *B*-spline fit) at three collision energies (11.0, 9.6, and 7.3 kcal/mol). For each collision energy, the LAB angle of the corresponding center of mass is indicated with a vertical dashed line. The speeds of the F_2 beam are 1525, 1360, and 1020 m/s, respectively, and the speed of the d6-DMS beam is maintained at 1210 m/s.

7.3 kcal/mol is much weaker because this collision energy is close to the threshold of channel II. More importantly, in this energy range, the reaction cross section[2] varies substantially within the spread of the collision energy (about ±0.8 kcal/mol). This effect leads to a strong correlation between the product recoil velocity and the reactant velocities. Our present forward convolution program cannot include this correlation yet. Consequently, for a collision energy near the reaction threshold, e.g., 7.3 kcal/mol, we have less confidence for the deduced energy distribution $P(E_T)$. At higher collision energies, this correlation problem is not severe anymore. For the angular distribution in the CM frame, the data still show clear feature of forward scattering at all collision energies in this study. The obtained $P(\theta_{CM})$ at 7.3 and 11 kcal/mol are quite similar with differences smaller than the experimental uncertainty. The scattering dynamics of channel II seems to depend rather weakly on the collision energy, in contrast to its branching ratio. Another evidence for this conclusion can be seen in Fig. 7(b), which shows the typical LAB-frame angular distributions of channel II products at three collision energies (7.3, 9.6, and 11 kcal/mol). All three curves are asymmetric with respect to the LAB angle of the center of mass. Their relative shapes are quite similar after considering the offsets due to the different LAB angles of the center of mass. This result indicates that the CM-frame angular distribution varies little in the range of the studied collision energies.

To interpret the results of channel II, it is important to mention that channels II and I are in competition. Near the threshold of channel II, most of the reactive flux leads to channel I products. It is reasonable to expect that the long-

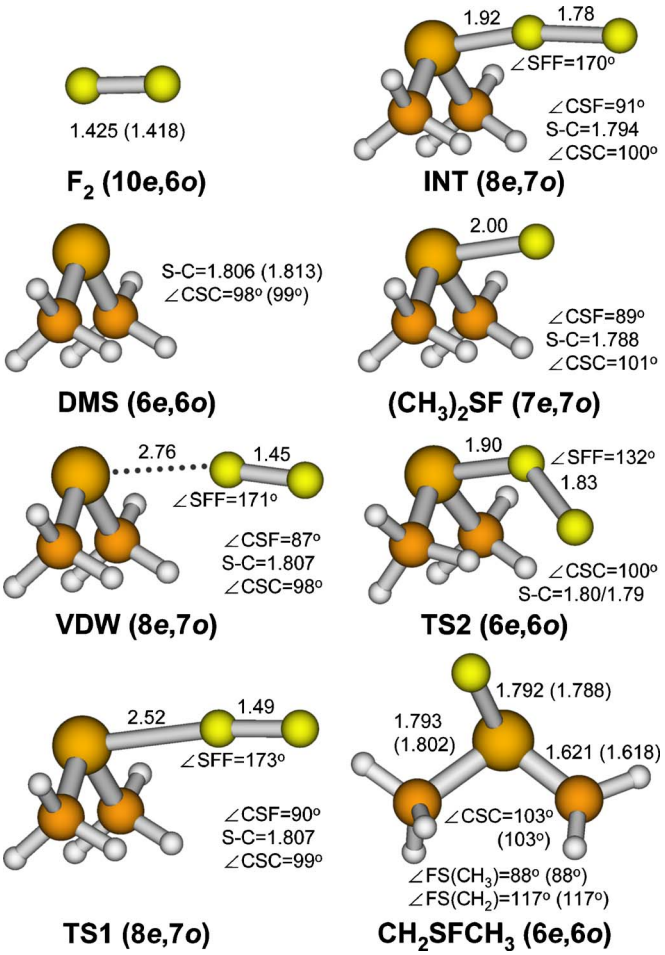

FIG. 8. (Color online) Optimized CASPT2 structures of F_2, DMS, van der Waals entrance well (VDW), transition states (TS1, TS2), intermediate (INT), and products. Selected bond distances (in Å) and angles (in degrees) are shown. The active spaces used in each optimization are denoted as (*ne*, *mo*) [*n* electrons distributed in *m* orbitals]. The QCISD(T) values (if applicable) are shown in parenthesis.

lived component of the collision complex population undergoes more complete intramolecular vibrational energy redistribution. If this energy randomization process is nearly complete, channel I should predominate over channel II because of much smaller energy required for this process (see Ref. 2 and next section). That is, only the short-lived component of the collision complex population has a probability to contribute to channel II. This may explain why the $P(\theta_{CM})$ of channel II does not show significant dependence on the collision energy within the range from 7.3 to 11 kcal/mol. Without further theoretical reactive scattering simulations, we can only qualitatively conclude that the angular distributions of both channel I and II are consistent with the short-lived complex model mentioned above.

B. *Ab initio* calculations

Figure 8 shows the optimized structures of DMS, van der Waals entrance-well complex (VDW), intermediate (INT), transition states (TS1, TS2), and the products obtained from the CASPT2 calculations. We believe that the CASPT2 method is capable to provide good equilibrium geometries for all the studied species provided that the active

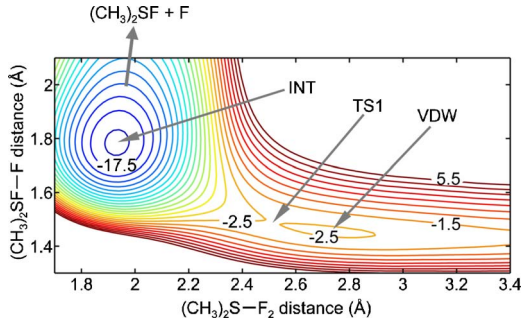

FIG. 9. (Color online) 2D CASPT2 potential energy surface for the entrance valley and INT of the F_2+DMS reaction. The numbers indicate the potential energy relative to the reactants in kcal/mol. The contour spacing is 1 kcal/mol. The inactive geometrical variables are fixed at the optimized TS1 structure.

spaces are carefully chosen and tested.[30] In the situations where the QCISD(T) analytical gradients are available, QCISD(T) has been used to confirm the CASPT2 equilibrium geometries. Our results—given in Fig. 8—show that these geometries are very similar for F_2, DMS, HF (R_e^{CASPT2}=0.931 Å; $R_e^{QCISD(T)}$=0.926 Å), and CH_2SFCH_3.

Following the scheme given in Ref. 2, the minimum energy paths can be schematically written as

$$F_2 + DMS \rightarrow VDW \rightarrow TS1 \rightarrow INT,$$

$$INT \rightarrow TS2 \rightarrow \text{channel I products},$$

$$INT \rightarrow \text{channel II products}.$$

For the path corresponding to channel II, the arrangement of the methyl groups in DMS, VDW, TS1, INT, and $(CH_3)_2SF$ is very similar (see Fig. 8), which indicates a spectatorlike character of the CH_3 groups. The change of the S-F-F angle along the reaction path is also small. The most important coordinates are clearly the S-F and F-F distances. To visualize the potential energy surface (PES) in this region, we have performed a two-dimensional (2D) energy scan spanned by these two coordinates. All other geometrical parameters are assumed to be identical to those in the TS1 structure. The resultant PES, shown in Fig. 9, gives the following direct conclusions: (i) attractive character of the entrance well is observed even for very long S-F distance, (ii) the energy barrier separating VDW and INT is negligible, and (iii) the reaction coordinate connecting INT and channel II products is almost identical to the F-F coordinate. The last observation suggests that the channel II products can be formed by simple F-F bond fission. We have extensively tested many active spaces from $(4e,3o)$ to $(10e,11o)$ in order to provide a smooth and reliable description of the reaction path near TS1. There are a few practical issues concerning proper use of active space in multireference calculations. The first issue concerns the problem of orbital switching, which refers to a rotation of two (or more) orbitals between the closed/active/virtual CAS subspaces. Very often such a switch leads to discontinuous PES. It can usually be avoided if a different set of starting orbitals or a slightly modified geometry is used as the input. The second issue concerns locating all chemically important molecular orbitals and including them in the

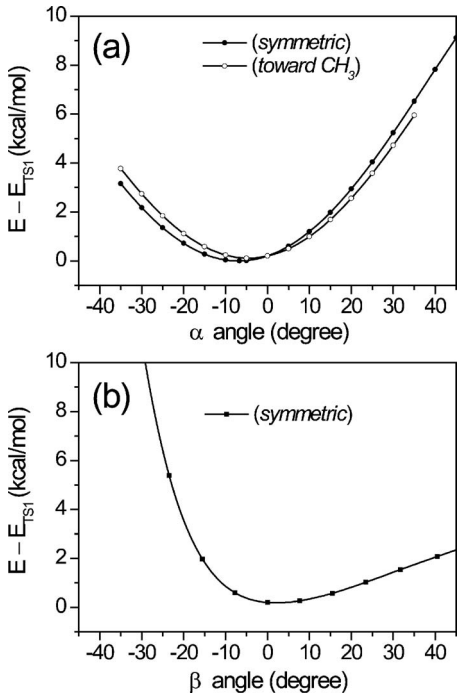

FIG. 10. CASPT2/$(8e,7o)$ potential energy curves for the TS1 structure as a function of bending angles: (a) between the S-F and the F-F bonds and (b) between the F-F-S axis and the normal to the C-S-C plane. The remaining geometry parameters are kept fixed. Negative value of the angle corresponds to a shorter distance to the center of the two C atoms (denoted as *symmetric*) or to one of the C atoms (denoted as *toward* CH_3).

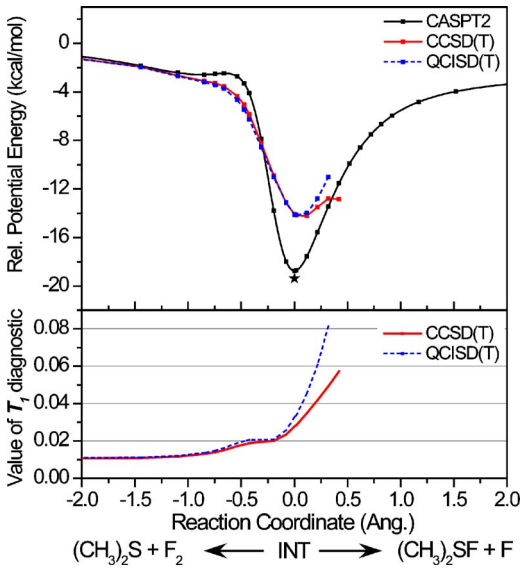

FIG. 11. (Color online) Relative potential energy curves along the minimum energy path determined from the 2D PES scan shown in Fig. 9. The geometry of the CH_3SCH_3 subsystem is fixed at the optimized TS1 structure. For INT, the energy corresponding to fully optimized structure is marked with a star. The values of the T_1 diagnostic for the CCSD(T) and QCISD(T) calculations are shown in the lower panel.

active space for all molecular structures on the PES. If the complications attributed to these two problems can be avoided, the resultant potential energy curves usually look smooth and resemble one another obtained with different active spaces.

Figure 10 shows one-dimensional energy scans along the bending angles α (upper panel) and β (lower panel), where α is defined as the angle between the F-F-S axis and the S-F bond, and β is defined as the angle between the F-F bond and the normal to the C-S-C plane. These scans suggest that TS1 structure is quite floppy except for the region where fluorine atoms undergo large steric hindrance from the methyl groups ($\beta<-20°$). The potential energy of the separated reactants is approximately 2.5 kcal/mol higher than that of TS1. It can be anticipated that the cone of acceptance for this reaction is quite wide even if the collision energy is negligible.

To further investigate this unusual reaction, we have computed single-point CCSD(T) and QCISD(T) energies for selected structures along the minimum energy path on the 2D PES (Fig. 9). The resultant CCSD(T) and QCISD(T) curves are shown in Fig. 11 together with the CASPT2 curve. Although the CCSD(T) and QCISD(T) calculations do not support the existence of TS1, they still confirm that this reaction is barrierless. In practice, these different shapes of PES around TS1 are not crucial for discussing the reaction mechanism, since the predicted energies at the TS1 structure are all significantly lower than the energy of the reactants. All the three curves presented in Fig. 11 give similar predictions on the energy landscape for the entrance valley, yet the predicted CASPT2 stabilization energy for INT is approximately 4.6 kcal/mol larger than for CCSD(T) and QCISD(T).

The single-reference based methods, such as CCSD(T) and QCISD(T), are capable to predict reaction energetics very accurately provided that the electronic structure of all the studied species can be reasonably well described by a single Slater determinant.[30–32] The quality of the single-reference correlation methods can be tested with the value of the T_1 diagnostic. The use of T_1 as a diagnostic is based on an empirical observation: the larger the T_1 value, the less accurate are molecular structures, binding energies, and vibrational frequencies obtained with the CCSD method.[31,32] A critical value of the T_1 diagnostic proposed by Lee *et al.*[32] is 0.02; if the actual calculated value is larger than 0.02, it suggests that the system may not be well described by the CCSD wave function. In the lower panel of Fig. 11, we present the value of the T_1 diagnostic computed with CCSD(T) and QCISD(T) along the reaction path. T_1 is quite small at the reactant valley and VDW. It slightly increases at TS1, but is still less than 0.02. After the reaction crosses the INT structure, T_1 increases rapidly. Consequently, the failure of the CCSD(T) and QCISD(T) calculations can be anticipated and the results of these two methods start to differ significantly. At INT, T_1 for CCSD(T) is about 0.028, not much larger than the critical value of 0.02. We believe that this value still allows us to use the single-point CCSD(T) and QCISD(T) energies in this region, even though their precision may be lower. We have also found that CCSD(T) and QCISD(T) cannot predict reliable geometries and vibrational frequencies for INT, owing to large errors in energy gradients associated with large variation of T_1 for minor changes in geometry. The presented results constitute a convincing

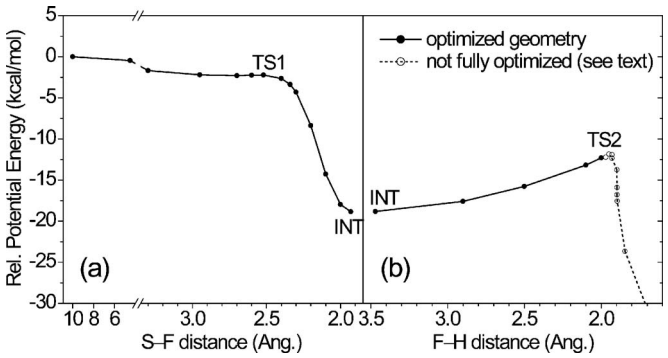

FIG. 12. CASPT2 energy curves along the minimum energy path (a) from the reactant valley through TS1 to INT and (b) from INT through TS2 towards the products of channel I. See text for details.

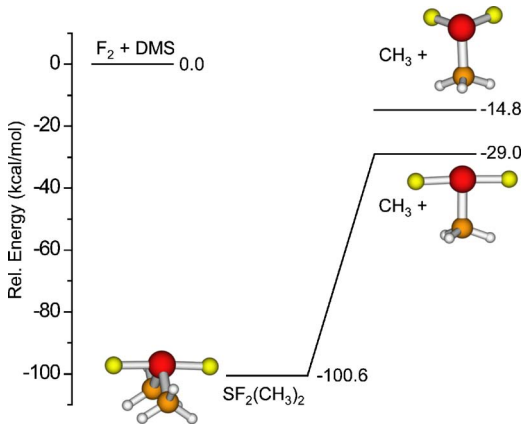

FIG. 13. (Color online) Schematic energy diagram (zero-point energy corrections included) shows possible decomposition pathways of $SF_2(CH_3)_2$. Geometry optimization and vibrational frequency calculation are performed with B3LYP using the basis sets: C,H=cc-pVDZ; S=cc-pV(T+d)Z; and F=aug-cc-pVTZ. Energy calculation is done with CCSD(T) using the basis sets: C,H=cc-pVDZ; S=cc-pV(Q+d)Z; and F=aug-cc-pVQZ.

evidence that the CASPT2, CCSD(T), and QCISD(T) calculations are capable of giving fairly accurate energy profile for the entrance valley of the studied reaction.

Locating the reaction path from INT to the HF $+CH_2SFCH_3$ products (channel I) has proved to be a nontrivial computational task. Our first approach—based on a constrained $(6e,6o)$ CASPT2 geometry optimization along the F–H distance—has not yielded a smooth energy curve due to a crossing of two electronic states near TS2. To avoid this problem, we have performed two-state CASSCF calculations at the one-state CASPT2 optimized geometries (solid circles in Fig. 12) along the F–H coordinate larger than 2.0 Å. For shorter distances of the F–H coordinate, two-state CASSCF calculations have been performed at geometries (open circles in Fig. 12) selected in a way that ensures formation of the HF product. The resultant ground-state CASSCF orbitals have been subsequently used to determine the one-state CASPT2 energy for every structure along the reaction path. Note that this procedure does not provide us with the minimal energy curve, but allows for finding an upper bound to it. The results are shown in Fig. 12, together with the potential energy curve from the reactant valley to INT calculated in the same way. The geometry optimization has been performed using the following selection of basis sets: cc-pVDZ for carbon and hydrogen, cc-pV(T+d)Z for sulfur, and aug-cc-pVTZ for fluorine. The single-point energy calculations can be performed with larger basis sets: cc-pVTZ, cc-pV(Q+d)Z, and aug-cc-pVQZ, respectively. It has been found that the size of the basis sets has only little effect on the relative energies. The TS2 barrier determined using the procedure described above is approximately 7.0 kcal/mol higher than the energy of INT. Calculations with other active spaces, e.g., $(8e,10o)$ or $(10e,9o)$, give similar results. Note that the value of 7.0 kcal/mol is only an upper-bound CASPT2 estimate for the barrier height; the barrier evaluated with fully optimized geometries would be slightly lower. The single-point CCSD(T) and QCISD(T) calculations give slightly lower values for the TS2 barrier height but the values of T_1 diagnostic are quite large [about 0.045 for CCSD(T)] indicating that these single-reference-based methods can be less reliable. These results can be summarized shortly as (i) a reaction path connecting INT and the $HF+CH_2SFCH_3$ products has been found; (ii) the structure of TS2 has been approximately located; and (iii) the energy of TS2 is significantly lower than the energy of reactants.

From the presented theoretical investigations, we can see that the INT is an important structure for the reaction. It has been speculated[12] that a charge-transfer mechanism of forming an ion pair, $[CH_3SCH_3]^+[F_2]^2$, can explain the unusually large reactivity between the two closed-shell reactants of F_2 and DMS. In this mechanism, the electron transfer is assumed to take place at a critical distance, at which the ionic potential energy curve crosses the neutral potential energy curve. For F_2+DMS reaction, the critical distance between the positive and negative charges can be calculated to be 2.5 Å, assuming the neutral potential energy curve is flat.[33] However, the separation of 2.5 Å is already in the range of repulsive interactions[34] between DMS and a molecule of a size similar to F_2. Although the proposed charge-transfer mechanism qualitatively explains the relative response of a class of compounds in the fluorine-induced chemiluminescence detector,[12] we think that such a picture is oversimplified. The Mulliken population analysis performed for our CASSCF wave functions indeed indicates a partial charge transfer from sulfur to fluorine atoms. However, the amount of the transferred charge seems to be too small to support the charge-transfer mechanism. In the view of molecular orbital theory, the observed chemical stability of INT originates rather from a coupling between the doubly occupied nonbonding orbital on sulfur and the σ/σ^* orbitals on the F_2 molecule. This picture can possibly be generalized to reactions of F_2 with other molecules having a loosely bound electron pair. If the lone pair of electrons of a molecule is more diffuse, the molecule should have higher reactivity toward F_2.

It has been mentioned in Ref. 2 that INT is not the most stable structure among the $C_2H_6SF_2$ isomers. The compounds with four-coordinated sulfur and both F atoms directly connected to the S atom are much more stable. For example, the $SF_2(CH_3)_2$ structure shown in Fig. 13 is more stable than INT by at least 80 kcal/mol. If any of such stable isomers is formed in the F_2+DMS reaction, we may antici-

pate the following experimental observations. First, such a stable intermediate should be long lived and the product angular distribution should be forward-backward symmetric. Furthermore, a dissociation of the S–C bond and formation of $CH_3+SF_2(CH_3)$ products should be very likely to occur, because there is no exit barrier and the available energy is quite high (see Fig. 13 for details). In our experiments, we observe no evidence for such hypothetical events, indicating that the $SF_2(CH_3)_2$ and other analogous low-energy isomers are not formed. We believe the reason is that these low-energy structures are not connected to the reactants by any kinetically favored reaction paths on the PES.

High level *ab initio* calculations predict that there is no entrance barrier for this reaction and an intermediate (INT) can be formed. Another important factor responsible for observing the reaction products is the exit barrier and/or endothermicity. As can be seen from Fig. 12, the potential energy of TS2 is significantly lower than the energy of reactants. The vibrational zero-point energy (ZPE) correction to TS2 is not significant [ΔZPE$=+0.83$ kcal/mol at the $(6e,6o)$ CASPT2 level]. These results indicate that the channel I products can be formed without any activation energy.

Similarly to most barrierless reactions, e.g., radical-radical recombination process, the dynamical bottleneck for these reactions usually occurs at large separations between the reactants.[30] Owing to a more significant effect of the long range attractive force at low collision energies, the reaction cross section may become smaller for higher collision energies. The experimental cross section—shown in Fig. 1 of Ref. 2—shows a clear trend for larger reaction cross sections at lower collision energies, which is consistent with the theoretical predictions presented here.

For higher collision energies, the experimental data (Fig. 2 of Ref. 2) indicates that the endothermic channel II can compete with channel I. Because the required energy for the channel I process is much lower than for channel II, the channel I products should predominate if the lifetime of INT is sufficiently long to permit complete energy randomization. However, the presented experimental results indicate that the lifetime is shorter than one rotational period. The experimental yield of channel II increases rapidly with the collision energy. These observations suggest that the steric factor might be much larger for channel II to allow the competition with the more energetically favorable channel I. The presented theoretical calculations support this deduction of mechanism, since the structural change in the $(CH_3)_2S$ subsystem is almost negligible for the channel II process.

Table I shows the summary of the computed energetics for the F_2+DMS reaction. The presented results are obtained from single-point CCSD(T) energy calculations performed at optimized CASPT2 structures. The ΔZPE are determined from the computed CASPT2 vibrational frequencies (not scaled). If the QCISD(T) method is applicable, it is used to confirm the CASPT2 results. From the results presented in Table I, we can draw the following conclusions: (i) ΔZPE plays only a minor role in the calculated energetics; (ii) relative energies depend only slightly on the employed basis sets; and (iii) small variation of the computed relative energies on the size of the basis sets suggests that the accuracy for the complete basis set limit (CBSL) extrapolation should be relatively high. For channel II, the CBSL extrapolation scheme follows a standard procedure suggested in literature, i.e., the Hartree-Fock energies are extrapolated with an $\exp(-\gamma_1 N)$ function and the correlation energies are extrapolated with a $\gamma_2 N^{-3}$ function,[35] where $N=3$, 4, and 5 for triple-, quadruple-, and quintuple-zeta basis sets, respectively. We have tested this procedure for the F_2 and SF molecules at several bond distances and found that the above two functions indeed fit the Hartree-Fock and CCSD(T) correlation energies very well for $N=3$, 4, 5, and 6. Since for INT and channel II, both the CH_3 groups have merely a spectatorlike character, a three-point $(N=3,4,5)$ extrapolation has been performed only with respect to the basis sets on sulfur and fluorine. When calculating the reaction enthalpy of channel I, one of the CH_3 groups is no longer a spectator. Therefore, a two-point $(N=3,4)$ interpolation has been used with basis sets of triple- and quadruple-zeta quality for all atoms. It has been found that a single $\gamma N^{-3.3}$ function is capable to predict very similar results as the two function [$\exp(-\gamma_1 N)$ and $\gamma_2 N^{-3}$] extrapolation discussed above. We have tested the validity of the single function extrapolation for a number of molecules (HF, F_2, SF, CH_3SF, H_2CS, $(CH_3)_2SF$, HN_3, HNCO, HN_3^+, $HNCO^+$). The best estimated reaction enthalpy $\Delta H^0_{0\ \mathrm{K}}$ of channel II is +3.4 kcal/mol, which is consistent with the experimental value of 4.2 ± 0.5 kcal/mol determined from the threshold of collision energy.[2] The $\Delta H^0_{0\ \mathrm{K}}$ of both channels obtained in this work is also consistent with our earlier work[2] in which the standard cc-pVNZ basis sets were used for all the atoms.

IV. SUMMARY

A detailed experimental and theoretical investigation of the barrierless reaction between F_2 and DMS is presented. Two reaction channels, denoted as I and II, have been observed and identified as primary product channels. Their translational energy and angular distributions at wide range of collision energies have been determined and discussed. The analysis of the angular distributions suggests that the reaction mechanism involves a short-lived intermediate. High level *ab initio* calculations confirm the experimental finding of negligible barrier height for this reaction. More detailed characterizations for the entrance region of the reaction have been performed with the PES calculated on the $F-FS(CH_3)_2$ and $FF-S(CH_3)_2$ coordinates and a few bending angles related with the incoming F_2 orientation. Three high-level *ab initio* methods, CASPT2, CCSD(T), and QCISD(T), have been used to probe the potential energy curve along the reaction coordinates. More suitable types of basis sets have been employed to improve the efficiency and accuracy of the calculation; the overall results are consistent with those obtained with the standard cc-pVNZ basis sets.[2] The F_2+DMS reaction features a weakly bound $F-F-S(CH_3)_2$ intermediate, which is short-lived with respect to rotation and decays competitively to channels I and II. The calculated reaction enthalpy of channel II is consistent with the experimental value. The structure of TS2 has

TABLE I. Summary of the calculated CCSD(T) and zero-point energies for channel I and II.

	Energy (Hartree)[a]					Relative Energy[f] (kcal/mol)	
	Channel II						
(N_C, N_H, N_S, N_F)	DMS	F_2	INT	$(CH_3)_2SF$	F	ΔH (INT)	ΔH (II)
(3,3,3,3)[b]	−477.4091	−199.3136	−676.7442	−577.0898	−99.6277	−12.12[g]	3.08
(3,3,4,4)	−477.4276	−199.3657	−676.8146	−577.1348	−99.6527	−11.99[g]	3.45
(3,3,5,5)	−477.4351	−199.3838		−577.1516	−99.6615		3.49
CBSL[c]	−477.4407	−199.3988		−577.1652	−99.6686		3.44
						ΔZPE	
ZPE_{CASPT2}[d]	0.0765	0.0020	0.0807	0.0783		1.36	−0.18
$ZPE_{QCISD(T)}$	0.0757	0.0021					
	Channel I						
	DMS	F_2		CH_2SFCH_3	HF		ΔH (I)[h]
(3,3,3,3)	−477.4091	−199.3136		−576.4949	−100.3490		−77.34
(4,4,4,4)	−477.4521	−199.3657		−576.5647	−100.3770		−78.99
CBSL[e]	−477.4792	−199.3986		−576.6088	−100.3947		−80.11
							ΔZPE
ZPE_{CASPT2}				0.0671	0.0094		−1.29
$ZPE_{QCISD(T)}$				0.0664	0.0093		−1.25

[a]Calculated at optimized CASPT2 geometries as shown in Fig. 8.
[b](N_C, N_H, N_S, N_F) denotes the selected basis sets as C=cc-pVN_CZ; H=cc-pVN_HZ; S=cc-pV(N_S+d)Z; F=aug-cc-pVN_FZ.
[c]CBSL=complete basis set limit. The Hartree-Fock energies were extrapolated with a function of $\exp(-\gamma_1 N)$; the correlation energies were extrapolated with a function of $\gamma_2 N^{-3}$, where $N=N_S=N_F$ and $N_C=N_H=3$.
[d]ZPE=vibrational zero-point energy. We have used the following basis sets: C,H=cc-pVDZ; S=cc-pV(T+d)Z; F=aug-cc-pVTZ, and active spaces: DMS=(6*e*,6*o*); F_2=(10*e*,6*o*); INT=(8*e*,7*o*); $(CH_3)_2SF$=(7*e*,7*o*); CH_2SFCH_3=(6*e*,6*o*); HF=(8*e*,5*o*).
[e]The CCSD(T) energies are extrapolated with a function of $\gamma N^{-3.3}$, where $N=N_C=N_H=N_S=N_F$.
[f]$\Delta H=\Delta U+\Delta ZPE$. *U* is the electronic energy.
[g]Tentative value, see text.
[h]with ΔZPE_{CASPT2}.

been approximately located even though there is a curve crossing problem around the TS2 geometry.

The presented results have motivated us to investigate reactions of F_2 with other sulfur-containing molecules. Preliminary theoretical and experimental works on the reactions of F_2 with CH_3SH and CH_3SSCH_3 reveal similar features: (i) the theory predicts an analogous intermediate can be formed without a significant entrance barrier; (ii) product channels analogues to channel II have been measured experimentally. It is noteworthy to mention that a similar HF product channel has been detected in the F_2+CH_3SH reaction but it has not been observed in the $F_2+CH_3SSCH_3$ reaction. Instead, the CH_3SF+CH_3SF channel has been observed as the major product channel. Locating the corresponding transition state is under investigation. These combined experimental and theoretical studies suggest that the reactivity of F_2 with molecules containing a loosely bound electron pair can be a common phenomenon, even though the molecule possesses a closed-shell electronic structure.

ACKNOWLEDGMENTS

National Science Council (Grant Nos. NSC95-2113-M-001-041-MY3 and NSC96-2113-M-009-022-MY3) and Academia Sinica, Taiwan supported this work. We thank Professor Yuan T. Lee for valuable comments and National Synchrotron Radiation Research Center, Taiwan for use of facilities.

[1] http://kinetics.nist.gov
[2] Y.-J. Lu, L. Lee, J.-W. Pan, H. A. Witek, and J. J. Lin, J. Chem. Phys. **127**, 101101 (2007).
[3] C. A. Ramsden, Chem. Soc. Rev. **23**, 111 (1994).
[4] J. M. Farrar and Y. T. Lee, J. Am. Chem. Soc. **96**, 7570 (1974).
[5] J. M. Farrar and Y. T. Lee, J. Chem. Phys. **63**, 3639 (1975).
[6] M. J. Coggiola, J. J. Valentini, and Y. T. Lee, Int. J. Chem. Kinet. **8**, 605 (1976).
[7] J. J. Valentini, M. J. Coggiola, and Y. T. Lee, J. Am. Chem. Soc. **98**, 853 (1976).
[8] J. J. Valentini, M. J. Coggiola, and Y. T. Lee, Faraday Discuss. Chem. Soc. **62**, 232 (1977).
[9] C. C. Kahler and Y. T. Lee, J. Chem. Phys. **73**, 5122 (1980).
[10] J. M. Farrar and Y. T. Lee, J. Chem. Phys. **65**, 1414 (1976).
[11] J. R. Grover, Y. Wen, Y. T. Lee, and K. Shobatake, J. Chem. Phys. **89**, 938 (1988).
[12] A. A. Turnipseed and J. W. Birks, J. Phys. Chem. **95**, 6569 (1991).
[13] J. Baker, V. A. Butcher, J. M. Dyke, and E. P. F. Lee, J. Phys. Chem. **99**, 10147 (1995).
[14] Y. T. Lee, Science **236**, 793 (1987).
[15] J. J. Lin, D. W. Hwang, S. Harich, Y. T. Lee, and X. Yang, Rev. Sci. Instrum. **69**, 1642 (1998).

[16] J. J. Lin, Y. Chen, Y. Y. Lee, Y. T. Lee, and X. Yang, Chem. Phys. Lett. **361**, 374 (2002).
[17] U. Even, J. Jortner, D. Noy, and N. Lavie, J. Chem. Phys. **112**, 8068 (2000).
[18] http://140.110.203.42/bldoc/21AU9WL.htm or www.nsrrc.org.tw
[19] P. Celani and H.-J. Werner, J. Chem. Phys. **112**, 5546 (2000).
[20] P. Celani and H.-J. Werner, J. Chem. Phys. **119**, 5044 (2003).
[21] T. H. Dunning, Jr., J. Chem. Phys. **90**, 1007 (1989).
[22] R. A. Kendall, T. H. Dunning, Jr., and R. J. Harrison, J. Chem. Phys. **96**, 6796 (1992).
[23] T. H. Dunning, Jr., K. A. Peterson, and A. K. Wilson, J. Chem. Phys. **114**, 9244 (2001).
[24] M. J. O. Deegan and P. J. Knowles, Chem. Phys. Lett. **227**, 321 (1994); P. J. Knowles, C. Hampel, and H.-J. Werner, J. Chem. Phys. **99**, 5219 (1993); J. Chem. Phys. **112**, 3106(E) (2000).
[25] G. Rauhut and H.-J. Werner, Phys. Chem. Chem. Phys. **3**, 4853 (2001).
[26] H.-J. Werner, P. J. Knowles, R. Lindh *et al.*, MOLPRO, Version 2006.1, a package of *ab initio* programs (http://www.molpro.net).
[27] R. D. Levine and R. B. Bernstein, *Reaction Dynamics and Chemical Reactivity* (Oxford University Press, 1987), pp. 411–417 and 104–113.
[28] G. A. Fisk, J. D. McDonald, and D. R. Hershbach, Faraday Discuss. Chem. Soc. **44**, 228 (1967).
[29] D. Troya, M. J. Lakin, G. C. Schatz, L. B. Harding, and M. González, J. Phys. Chem. B **106**, 8148 (2002).
[30] L. B. Harding, S. J. Klippenstein, and A. W. Jasper, Phys. Chem. Chem. Phys. **9**, 4055 (2007).
[31] T. J. Lee and G. E. Scuseria, in *Quantum Mechanical Electronic Structure Calculations with Chemical Accuracy*, edited by S. R. Langhoff (Kluwer, Dordrecht, 1995), pp. 47–108.
[32] T. J. Lee and P. R. Taylor, Int. J. Quantum Chem., Symp. **23**, 199 (1989).
[33] We calculated the Coulomb potential between the positive and negative ions using the values of IE(DMS)=8.7 eV and EA(F_2)=3.0 eV (IE=ionization energy and EA=electron affinity). The critical distance of 2.6 Å in Ref. 12 was calculated from a less accurate IE of DMS.
[34] The summation of the van der Waals radii (R_{VDW}) of one S atom (R_{VDW}=1.80 Å) and one F atom (R_{VDW}=1.47 Å) is about 3.27 Å, which is significantly larger than the critical distance of 2.5 Å. For van der Waals radii, see L. Pauling, *The Nature of the Chemical Bond* 3rd ed. (Cornell University Press, Ithaca 1960); A. Bondi, J. Phys. Chem. **68**, 441 (1964); J. K. Badenhoop and F. Weinhold, J. Chem. Phys. **107**, 5422 (1997). We use Bondi's values here. In addition, we have checked the repulsive interaction between DMS and neon; the potential energy [CCSD(T)/aug-cc-pVTZ] at 2.5 Å of the Ne–$S(CH_3)_2$ distance is about 7–9 kcal/mol (orientation dependent) higher than the separated molecules. Because Ne (R_{VDW}=1.54 Å) and F have a similar van der Waals radius, such a neon probe may yield some information on the hypothetical DMS+F_2 repulsive interaction.
[35] T. Helgaker, W. Klopper, H. Koch, and J. Noga, J. Chem. Phys. **106**, 9639 (1997).